J Mater Sci (2022) 57:16367–16382

Electronic materials

Biocompatible polysaccharide ionic hydrogel as ultra-stretchable and multifunctional wearable sensor

Yuchen Zhou[1], Tianyi Dai[1], Yaqi Cheng[1], Qingchen Deng[1], Xueyu Li[1], Hao Wu[2], Wenjiao Han[3], and Hongbing Jia[1,*]

[1] *Key Laboratory for Soft Chemistry and Functional Materials of Ministry of Education, Nanjing University of Science and Technology, Nanjing 210094, China*

[2] *School of Biomedical Engineering and Informatics, Department of Biomedical Engineering, Nanjing Medical University, Nanjing 211166, China*

[3] *School of Energy and Power Engineering, Nanjing University of Science and Technology, Nanjing 210094, China*

Received: 11 May 2022
Accepted: 11 August 2022
Published online: 30 August 2022

ABSTRACT

Due to their promising applications in health monitoring, wearable flexible sensors based on hydrogel have gained considerable attention as modern medicine advances. However, it is still challenging for hydrogel-based wearable flexible sensors to be integrated with high stretchability, multifunctionality, and biocompatibility. Herein, we designed novel flexible multifunctional sensors based on ionic conductive double-network (DN) hydrogels composed of poly (acrylamide-*co*-acrylic acid) (P(AM-*co*-AAc)), sodium alginate (SA), and calcium chloride ($CaCl_2$) by simple two-step method of copolymerization and soaking. Abundant carboxyl groups on SA and P(AM-*co*-AAc) chains and their capacity to bind with Ca^{2+} were utilized to design a double network, providing the hydrogels with high stretchability and toughness. Ca^{2+} endowed the hydrogels with enhanced conductivity and sensitivity, while P(AM-*co*-AAc) enabled the hydrogels to respond to multi-stimuli. The SA/P(AM-*co*-AAc)/Ca^{2+} hydrogels presented outstanding mechanical properties (elongation at break of 2626%, tensile strength of 372 kPa), great sensitivity (gauge factor up to 7.1), and excellent durability (1000 stretching-releasing cycles). It could detect human movements, touch, physiology (temperature and sweat), pH changes, and organic solvents. Besides, the hydrogel sensors displayed great biocompatibility. Therefore, this work extends the design and preparation of highly stretchable and multifunctional hydrogels to facilitate the applications of skin-friendly wearable sensors.

Handling Editor: Chris Cornelius.

Address correspondence to E-mail: polymernjust@gmail.com

https://doi.org/10.1007/s10853-022-07635-5

GRAPHICAL ABSTRACT

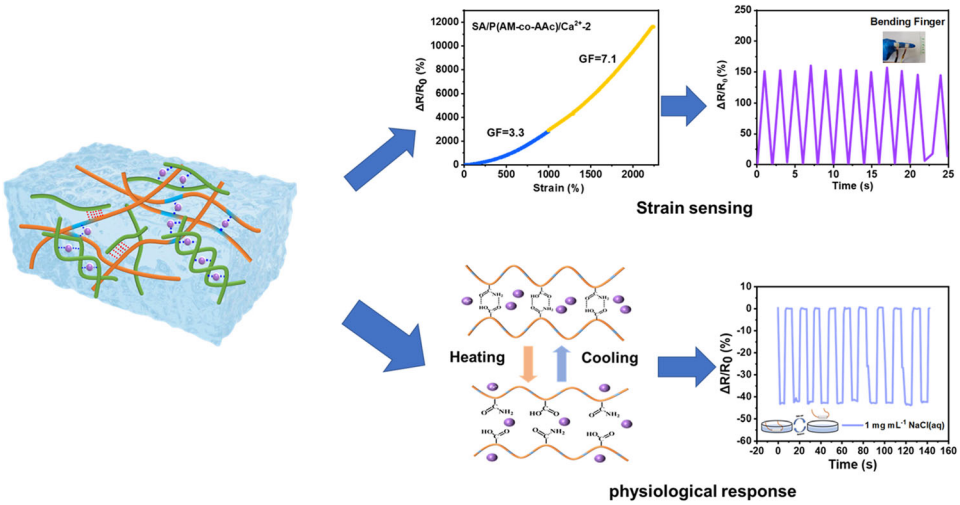

Introduction

Recently, flexible strain sensors, which can transform physical signals into electrical signals, have attracted widespread attention for their extensive applications in health monitoring [1, 2], soft robots [3, 4], and many other aspects [5, 6]. Due to the unique combination of mechanical flexibility and conductivity [7–9], ionic conductive hydrogels have become ideal materials for wearable strain sensors. For example, Tie [10] prepared strain sensors composed of polyacrylamide (PAM), polyvinyl alcohol acetoacetate (PVAA), and Fe^{3+}, which could be used as potential artificial ionic skins to monitor human motions. However, most ionic conductive hydrogel sensors suffer from weak sensitivity, poor mechanical properties and only respond to a single stimulus such as strain–stress changes, which limits their practical applications. Therefore, the preparation of hydrogel sensors with excellent sensitivity, high mechanical properties, and the capacity to respond to multiple stimuli is of great significance.

Recently, hybrid double-network hydrogels with physical and chemical networks were reported to exhibit super toughness and excellent self-recovery performance due to the reversible interruption and re-crosslinking of the physical network [11]. For example, Xia [12] developed highly stretchable chitosan (CS)/Al^{3+}-PAM DN hydrogel by integrating a physical CS network coordinated with Al^{3+} and a chemically crosslinked PAM network. The obtained sensors possessed great mechanical properties (tensile strength of 264.3 kPa, elongation at break of 2173.9%), rapid self-recoverability, and favorable fatigue resistance. Therefore, the introduction of the physical crosslinking network in DN hydrogels is expected to improve the mechanical properties.

Poly (acrylamide-*co*-acrylic acid) (P(AM-*co*-AAc)) can respond to the changes in temperature, solvent polar, and pH [13] due to its characteristics of thermo-sensibility and polyelectrolyte. For example, our group [14] reported that poly (vinyl alcohol) (PVA)/P(AM-*co*-AAc)/Fe^{3+} sensors could detect human motions, physiological activities, and pH changes.

In this work, we designed DN hydrogel sensors based on sodium alginate (SA)/P(AM-*co*-AAc)/Ca^{2+} with excellent stretchability, great sensing sensitivity, multifunctionality, and biocompatibility. Acrylamide (AM) and acrylic acid (AAc) were copolymerized in the presence of SA to form SA/P(AM-*co*-AAc) hydrogels, which were subsequently immersed in $CaCl_2$/ethanol mixed solutions. Hydrogen bonds were formed between chains of SA and P(AM-*co*-AAc), while ionic cooperation was formed between

Ca^{2+} and carboxyl groups from both SA and P(AM-*co*-AAc). The obtained DN SA/P(AM-*co*-AAc)/Ca^{2+} hydrogel sensors displayed excellent mechanical properties (elongation at break of 2626%, tensile strength of 372 kPa), outstanding strain sensitivity (gauge factor (GF) of 7.1), and high durability (1000 stretching-releasing cycles). It could not only detect real-time physical movements but also respond to physiology (temperature and sweat) and other stimuli (including pH, and organic solvents). The hydrogel sensors also showed excellent biocompatibility, providing potential applications for wearable strain sensors.

Experimental sections

Materials

Sodium alginate (SA, AR grade) was purchased from Alfa Aesar Chemical Co., Ltd. (China). Acrylamide (AM, AR grade), acrylic acid (AAc, purity ≥ 99.5%, relative density 1.048–1.052), ammonium persulfate (APS) (purity ≥ 98%), ethanol (AR grade), and anhydrous calcium chloride were provided by Nanjing Chemical Reagent Co., Ltd.

Fabrication of SA/P(AM-*co*-AAc)/Ca^{2+} DN hydrogels

The two-step preparation of SA/P(AM-*co*-AAc)/Ca^{2+} DN hydrogels included polymerization and soaking. Firstly, different amounts of SA powders were dissolved in 24 mL of deionized water and stirred at room temperature for 1 h to obtain SA solutions (0.5, 1, and 2 wt%, respectively). Then, AM monomers (11.9 g) and AAc (240 mg) were added to the above solutions and stirred for 1 h continuously until the solutions were uniform. After that, APS (0.2 mol% of AM) was added to the solutions. After stirring and ultrasonic de-bubbling, the solutions were injected into polytetrafluoroethylene (PTFE) molds, and the SA/P(AM-*co*-AAc) hydrogels were prepared by heating in an oven at 60 °C for 6 h.

Subsequently, the obtained SA/P(AM-*co*-AAc) hydrogels were cut into rectangles shapes ($30 \times 10 \times 0.5$ mm^3) and then immersed into $CaCl_2$/ethanol mixed solutions with different Ca^{2+} concentrations (0.1, 0.3, 0.5 and 0.7 M) for 3 h to obtain SA/P(AM-*co*-AAc)/Ca^{2+} DN hydrogels.

The obtained hydrogels (0.3 M for Ca^{2+}) with SA content of 0.5, 1, and 2 wt% were dominated as 0.5%SA, 1%SA, and 2%SA, respectively. The obtained hydrogels (2 wt% SA) with Ca^{2+} concentrations of 0.1, 0.3, 0.5 and 0.7 M were dominated as SA/P(AM-*co*-AAc)/Ca^{2+}-1, SA/P(AM-*co*-AAc)/Ca^{2+}-2, SA/P(AM-*co*-AAc)/Ca^{2+}-3 and SA/P(AM-*co*-AAc)/Ca^{2+}-4, respectively. The specific compositions are presented in Table S1.

Fabrication of SA/P(AM-*co*-AAc)/Ca^{2+} strain sensors

After removing the surface water of SA/P(AM-*co*-AAc)/Ca^{2+} hydrogels, the SA/P(AM-*co*-AAc)/Ca^{2+} strain sensors were prepared by coating silver paste to both ends of the cuboid and fixing the copper wires with insulating tapes.

Measurements

The morphologies of SA/P(AM-*co*-AAc) and SA/P(AM-*co*-AAc)/Ca^{2+} hydrogels were characterized by scanning electron microscopy (SEM, Quanta 250 FEG, FEI). The structures of SA/P(AM-*co*-AAc) and SA/P(AM-*co*-AAc)/Ca^{2+} hydrogels were assessed via Fourier transform infrared (FTIR) spectrometer (FTIR-8400S, Shimadzu, Japan) ranging from 4000 to 400 cm^{-1}. The rheological properties of samples were tested by a rotary rheometer (MCR 301, Anton Paar, Austria). The mechanical testing of hydrogel samples was performed using a universal tensile testing machine (CMT 4254, Shenzhen Sansi Testing Co. Ltd., China) at room temperature with a humidity of 25%. The samples were cut into strips of $30 \times 10 \times 0.5$ mm^3. The tensile rate was 100 mm min^{-1}. The test results were averaged over five independent tests. The swelling tests were performed by cutting the hydrogels into rectangular shapes and immersing them in $CaCl_2$ solution and $CaCl_2$/EtOH solution. The weight of hydrogels was measured every 30 min. The swelling rate (SR) was defined as Eq. (1):

$$SR = \frac{W_s - W_0}{W_0} \times 100\% \quad (1)$$

where W_S was the weight of the swollen hydrogels, and W_0 was the weight of origin hydrogels.

The sensing property of strain sensors was characterized by a digital source meter (Keithley 2400, Tektronix Inc., US) and an electronic universal tensile testing machine (CMT 4254, Shenzhen Sansi Testing Co., Ltd., China) at a voltage of 3 V.

The biocompatibility of the hydrogels was evaluated by employing the MTT assay against HUVEC cells. Incubation of HUVEC cells was performed in Dulbecco's Modified Eagle's Medium (DMEM). Then, the HUVEC cells were transplanted to 96-well plates and treated with UV-sterilized hydrogels. A microplate reader was used to measure optical density (OD) at 450 nm to assess cell viability.

Result and discuss

Synthesize and characterization of SA/P(AM-*co*-AAc)/Ca^{2+} DN hydrogels

The fabrication mechanism of SA/P(AM-*co*-AAC)/Ca^{2+} DN hydrogels is illustrated in Fig. 1. Firstly, SA/P(AM-*co*-AAc) hydrogels were obtained by copolymerizing AM and AAc in the presence of SA (Fig. 1a, b). Hydrogen bonds were formed between SA and P(AM-*co*-AAc). Subsequently, the SA/P(AM-*co*-AAc) hydrogels were immersed in $CaCl_2$/ethanol mixed solvent to introduce Ca^{2+}. Ionic crosslinking was constructed due to the interaction of Ca^{2+} with carboxyl groups from both SA and P(AM-*co*-AAc) (Fig. 1c), which constructed the DN network and enhanced the mechanical properties of SA/P(AM-*co*-AAC)/Ca^{2+} hydrogels [15].

The FTIR spectra of SA, the mixture of SA, AM, and AAc, SA/P(AM-*co*-AAc) hydrogels, and SA/P(AM-*co*-AAc)/Ca^{2+} hydrogels were conducted (Fig. 2a). It could be seen that the FTIR spectrum of SA showed characteristic peaks at 3304 cm^{-1} (stretching vibration of O–H), 1616 cm^{-1} (antisymmetric stretching vibration of COO^-), 1413 cm^{-1} (symmetric stretching vibration of COO^-), and 1029 cm^{-1} (stretching vibration of C–O–C) [16]. For the mixture of SA, AM, and AAc before polymerization, there are peaks at 3342 cm^{-1} and 3195 cm^{-1} (stretching vibration of N–H), 1660 cm^{-1} (stretching vibration of C=O), 1625 cm^{-1} (stretching vibration of C=C), and 1439 cm^{-1} (asymmetric and symmetric

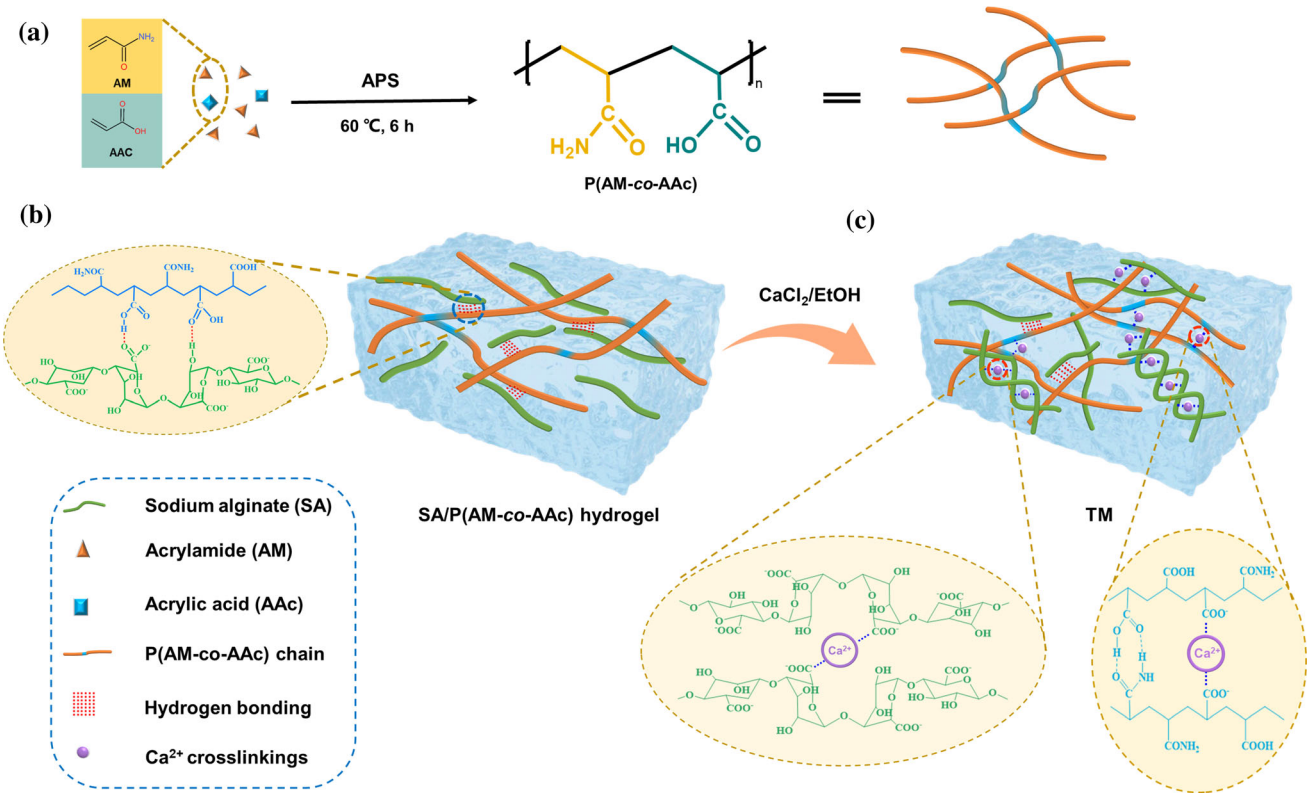

Figure 1 The fabrication mechanism of SA/P(AM-*co*-AAc)/Ca^{2+} hydrogels: **a** copolymerization of AM and AAc, **b** SA/P(AM-*co*-AAc) hydrogels, **(c)** SA/P(AM-*co*-AAc)/Ca^{2+} hydrogels.

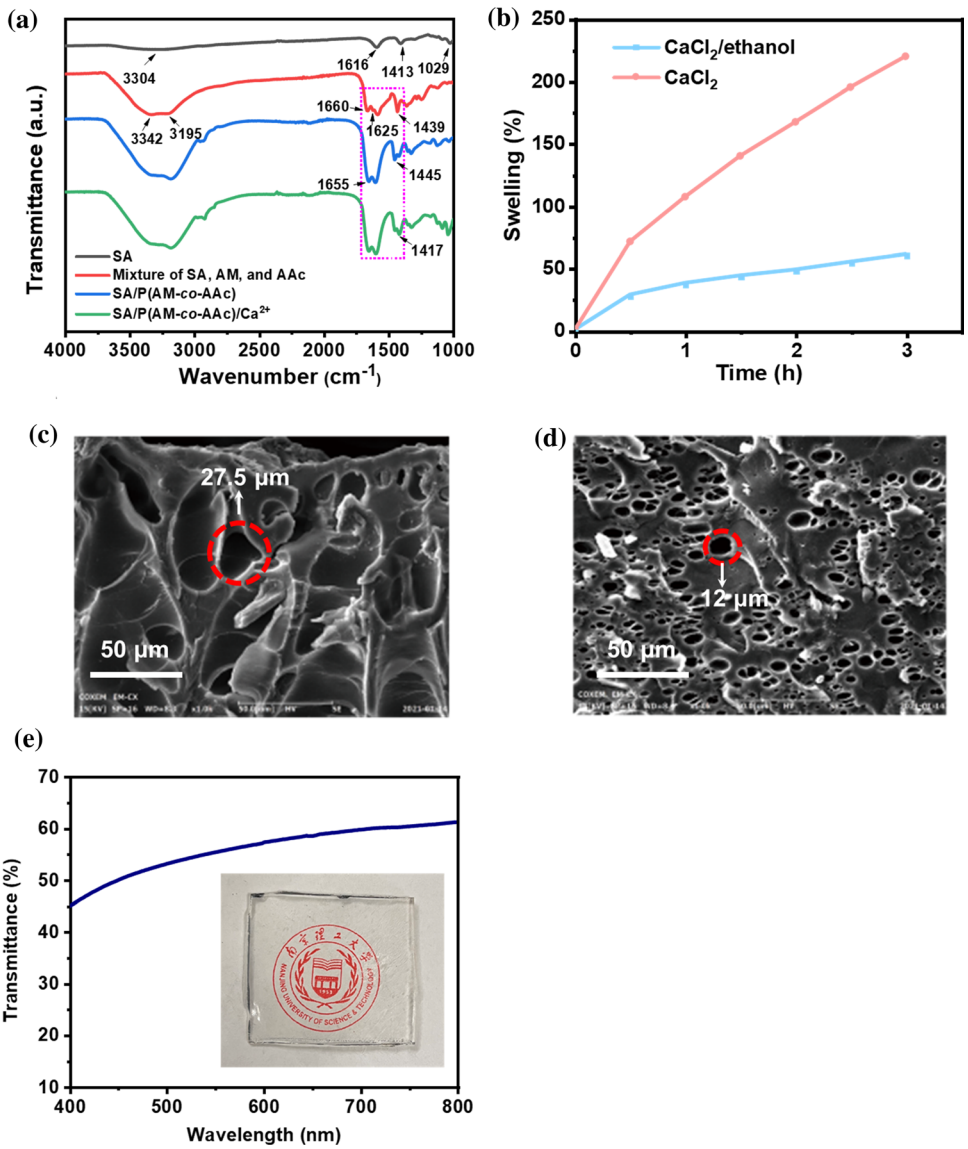

Figure 2 **a** FTIR spectra of SA, mixture of SA, AM, and AAc, SA/P(AM-*co*-AAc) hydrogels, and SA/P(AM-*co*-AAc)/Ca^{2+} hydrogels, **b** swelling ratios of SA/P(AM-*co*-AAc)/Ca^{2+} hydrogels in $CaCl_2$ and $CaCl_2$/EtOH solution, SEM images of **c** SA/P(AM-*co*-AAc) hydrogels and **d)** SA/P(AM-*co*-AAc)/Ca^{2+} hydrogels, **e** the transmittance spectrum of the SA/P(AM-*co*-AAc)/Ca^{2+} hydrogels (inset is the hydrogel thin sheet graph against the white background paper).

stretching vibration of COO^-), respectively. The disappearance of the stretching vibration of C=C in the SA/P(AM-*co*-AAc) FTIR spectrum indicated the occurrence of polymerization. After being immersed in $CaCl_2$/ethanol mixed solvents, the stretching vibration peak of COO^- (1445 cm^{-1}) of SA/P(AM-*co*-AAc) shifted to 1417 cm^{-1} in SA/P(AM-*co*-AAc)/Ca^{2+} hydrogel, displaying the ionic bond between Ca^{2+} and COO^- [17].

The swelling ratios of SA/P(AM-*co*-AAc) hydrogels in $CaCl_2$ solution and $CaCl_2$/ethanol solution were tested (Fig. 2b). It demonstrated that swelling ratios of SA/P(AM-*co*-AAc) hydrogels were lower in $CaCl_2$/ethanol solution than those in $CaCl_2$ solution. This phenomenon revealed that EtOH could decrease the swelling ratio of SA/P(AM-*co*-AAc) hydrogels [18].

SEM images of SA/P(AM-*co*-AAc) and SA/P(AM-*co*-AAc)/Ca^{2+} hydrogels are shown in Fig. 2c, d. It exhibits that SA/P(AM-*co*-AAc) hydrogels had relatively large, loose, and chaotic pores, while those of SA/P(AM-*co*-AAc)/Ca^{2+} hydrogels were small, dense, and ordered [19]. The introduction of Ca^{2+} not only increased the crosslinking points and stabilized the hydrogel structure, but also facilitated the shuttle of ions inside the hydrogel network, which provided the hydrogel with conductivity [20].

Transmittance is an index to measure esthetic visualization. The transmittance spectrum of SA/P(AM-*co*-AAc)/Ca^{2+} DN hydrogels was tested via

UV–Vis spectrophotometer (Fig. 2e). The highest light transmission rate of SA/P(AM-*co*-AAc)/Ca^{2+} DN hydrogels was 61%, which was beneficial for the data visualization of wearable products.

Mechanical properties of SA/P(AM-*co*-AAc)/Ca^{2+} hydrogels

The stress–strain curves of SA/P(AM-*co*-AAc)/Ca^{2+} hydrogels (0.3 M for Ca^{2+}) with different SA content are shown in Fig. 3a. It could be seen that both the tensile strength and elongation at break of SA/P(AM-*co*-AAc)/Ca^{2+} hydrogels improved with the increase in SA content. Hydrogen bonds formed by SA with P(AM-*co*-AAc) and ionic bonds formed by the carboxyl groups of SA with Ca^{2+} accounted for the growth of mechanical strength. The optimized hydrogels with 2 wt% SA had the best tensile strength (372 kPa) and elongation at break (2626%). Therefore, SA/P(AM-*co*-AAc)/Ca^{2+} hydrogels with 2 wt% SA were chosen for further studies.

The effects of Ca^{2+} concentrations on the mechanical properties of SA/P(AM-*co*-AAc)/Ca^{2+} hydrogels (2 wt% SA) were also investigated. As shown in Fig. 3b, the stress–strain curve of SA/P(AM-*co*-AAc) hydrogels had no obvious yield point during the tensile process, indicating that there was no formation of a crosslinked network inside. However, the mechanical properties of the hydrogels exhibited superior improvement after being immersed in $CaCl_2$/EtOH and increased with the increase in Ca^{2+} concentration. It was attributed to the crosslinking of Ca^{2+} between SA/P(AM-*co*-AAc) hydrogels [21]. The increase in Ca^{2+} concentrations promoted the crosslinking density of the hydrogels, thereby enhancing the mechanical properties of the hydrogels. SA/P(AM-*co*-AAc)/Ca^{2+}-4 displayed the highest tensile strength (441 kPa) and elongation at break (2924%). In addition, the SA/P(AM-*co*-AAc)/Ca^{2+} hydrogels presented an excellent capacity to maintain different large deformations (Fig.S1). It could be seen that the SA/P(AM-*co*-AAc)/Ca^{2+} hydrogels could withstand large deformations after stretching, knotting, and twisting, and could be stretched up to 5 times the original length without breaking under the above circumstances, indicating that the hydrogels had excellent flexibility.

The rheological tests of SA/P(AM-*co*-AAc)/Ca^{2+} hydrogels under 0.5% fixed strain were carried out (Fig. 3c, d). The storage modulus (G') for all samples was higher than the loss modulus (G'') over the whole angular frequency ranging from 1 to 100 rad s^{-1}, indicating that SA/P(AM-*co*-AAc)/Ca^{2+} hydrogels formed a stable crosslinked network and showed solid-like behavior [22]. Compared with SA/P(AM-*co*-AAc), the G' of SA/P(AM-*co*-AAc)/Ca^{2+} significantly improved, suggesting that the introduction of Ca^{2+} improved the strength of hydrogels due to the ionic crosslinking between Ca^{2+} and carboxyl groups from SA and P(AM-*co*-AAc) [23]. The G' of hydrogels improved with the increase in SA content and Ca^{2+} concentrations. It was consistent with the changing trend in the stress strain of SA/P(AM-*co*-AAc)/Ca^{2+} hydrogels.

Anti-fatigue and self-recovery are crucial for the durability of sensors. DN structure enables hydrogels to recover after deformation to improve fatigue resistance. Figure 3e, f manifests continuous cyclic tensile loading–unloading curves and the dissipated energy of SA/P(AM-*co*-AAc)/Ca^{2+}-2 at a fixed strain of 200%. The SA/P(AM-*co*-AAc)/Ca^{2+}-2 exhibited an observable hysteresis loop after the first stretch with the dissipated energy of 0.25 kJ m^{-3} (Fig. 3f). During the process of deformation, hydrogels were inclined to disrupt the dynamic reversible bonds to remain the polymer network stable [24]. After that, the hysteresis curves remained unchanged virtually. It presented that SA/P(AM-*co*-AAc)/Ca^{2+}-2 possessed excellent fatigue resistance and maintained stability during continuous cyclic tensile loading–unloading tests. Figure 3g, h presents the tensile loading–unloading curves of SA/P(AM-*co*-AAc)/Ca^{2+}-2 at 200% strain for four times cycles with 10-min rest in each cycle and the corresponding energy dissipation. Compared with Fig. 3e, f, there was no obvious hysteresis loop after 10-min rest (Fig. 3g) and the energy dissipation almost remained constant. This is due to the rebuilding of dynamic reversible bonds (ionic and hydrogen bonds) in the double-network structure after 10-min rest, improving the self-recovery performance of SA/P(AM-*co*-AAc)/Ca^{2+} DN hydrogels.

Sensing properties of the SA/P(AM-*co*-AAc)/Ca^{2+} sensors

Figure 4a illustrates the conductivity of SA/P(AM-*co*-AAc)/Ca^{2+} sensors. It could be seen that the increase in Ca^{2+} concentrations improved the conductivity of the SA/P(AM-*co*-AAc)/Ca^{2+} sensors. Figure 4b exhibits relationships between $\Delta R/R_0$ and Ca^{2+}

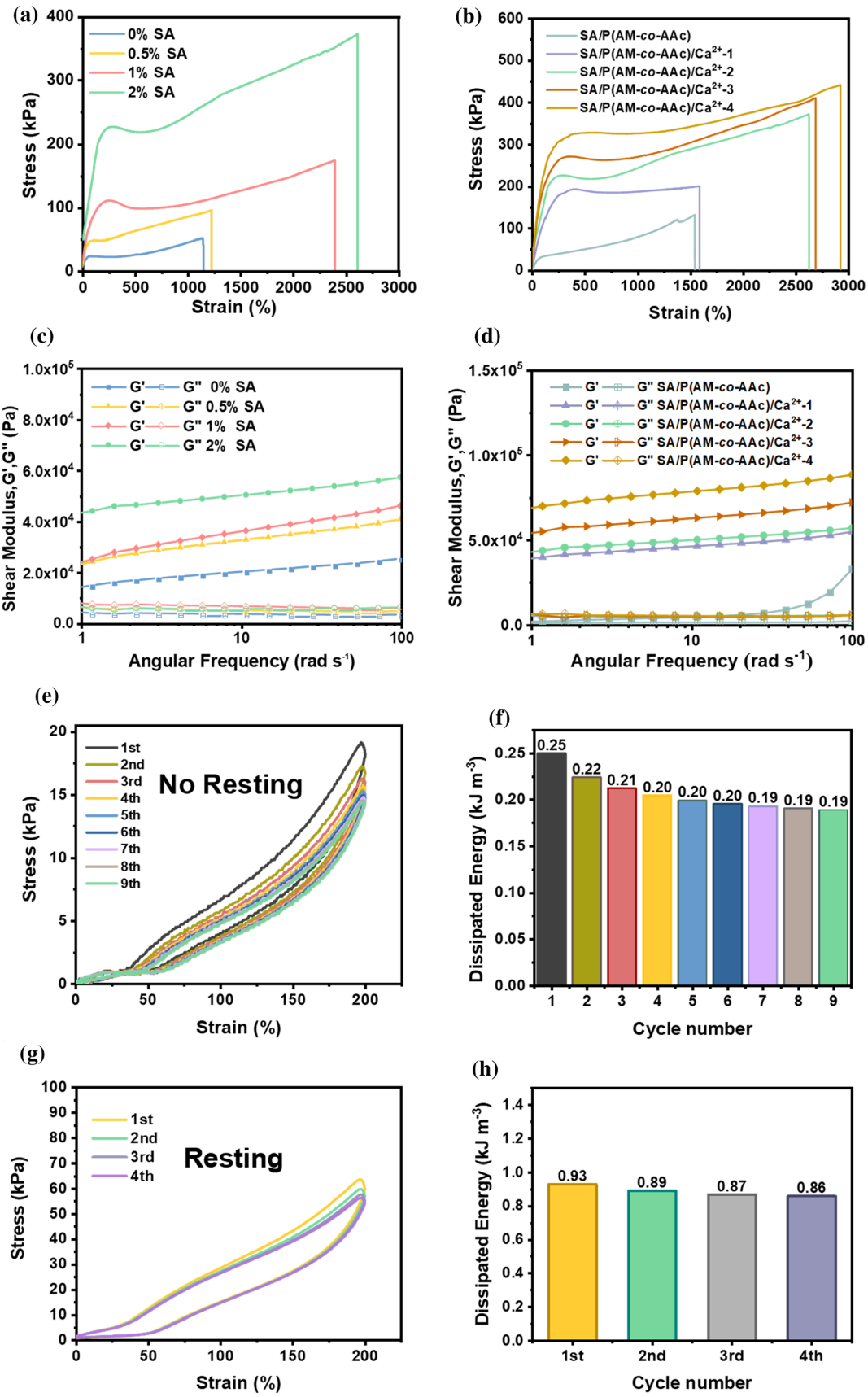
(a)
0% SA
0.5% SA
1% SA
2% SA
Stress (kPa)
Strain (%)
(b)
SA/P(AM-co-AAc)
SA/P(AM-co-AAc)/Ca2+-1
SA/P(AM-co-AAc)/Ca2+-2
SA/P(AM-co-AAc)/Ca2+-3
SA/P(AM-co-AAc)/Ca2+-4
Stress (kPa)
Strain (%)
(c)
G' G" 0% SA
G' G" 0.5% SA
G' G" 1% SA
G' G" 2% SA
Shear Modulus,G',G" (Pa)
Angular Frequency (rad s-1)
(d)
G' G" SA/P(AM-co-AAc)
G' G" SA/P(AM-co-AAc)/Ca2+-1
G' G" SA/P(AM-co-AAc)/Ca2+-2
G' G" SA/P(AM-co-AAc)/Ca2+-3
G' G" SA/P(AM-co-AAc)/Ca2+-4
Shear Modulus,G',G" (Pa)
Angular Frequency (rad s-1)
(e)
1st
2nd
3rd
4th
5th
6th
7th
8th
9th
No Resting
Stress (kPa)
Strain (%)
(f)
0.25
0.22
0.21
0.20
0.20
0.20
0.19
0.19
0.19
Dissipated Energy (kJ m-3)
Cycle number
(g)
1st
2nd
3rd
4th
Resting
Stress (kPa)
Strain (%)
(h)
0.93
0.89
0.87
0.86
Dissipated Energy (kJ m-3)
1st
2nd
3rd
4th
Cycle number

◀**Figure 3** Stress–strain curves of SA/P(AM-*co*-AAc)/Ca^{2+} hydrogels with **a** different SA content and **b** different Ca^{2+} concentrations, loss modulus and storage modulus of SA/P(AM-*co*-AAc)/Ca^{2+} hydrogels with **c** different SA content and **d** different Ca^{2+} concentrations, **e** continuous cyclic tensile loading–unloading curves of SA/P(AM-*co*-AAc)/Ca^{2+}-2 at 200% strain and **f** the energy dissipation, **g** continuous cyclic tensile loading–unloading curves of SA/P(AM-*co*-AAc)/Ca^{2+}-2 at 200% strain with 10-min rest and **h** the energy dissipation.

concentrations of the SA/P(AM-*co*-AAc)/Ca^{2+} sensors. $\Delta R/R_0$ of all samples increased with the applied strain. When the SA/P(AM-*co*-AAc)/Ca^{2+} sensors were stretched, the conductive ion channels extended and the migration of Ca^{2+} decreased. Hence, the conductivity resistance of SA/P(AM-*co*-AAc)/Ca^{2+} sensors increased [25]. On the other hand, the increase in Ca^{2+} concentrations improved the crosslinking density of the hydrogel network, making the hydrogel network less susceptible to damage under the same strain and reducing the diffusion of Ca^{2+}, leading to the decrease in $\Delta R/R_0$.

The sensing performance of the sensors is usually expressed by the gauge factor (GF). GF is calculated by the followed Eq. (2):

$$GF = (\Delta R/R_0)/\varepsilon \quad (2)$$

where ΔR means the resistance change at a certain strain level, R_0 is the initial resistance and ε represents the strain.

Figure 4c presents that GF values of SA/P(AM-*co*-AAc)/Ca^{2+}-2 sensors reached 7.1 when the strain was larger than 1000%. To intuitively highlight the trade-off of SA/P(AM-*co*-AAc)/Ca^{2+}-2, a comprehensive comparison of the properties of our hydrogel sensors with those reported in the literature is shown in Fig. 4d [26–34]. It can be seen that SA/P(AM-*co*-AAc)/Ca^{2+}-2 exhibits a great trade-off between high elongation at break, great strain sensitivity (Gauge factor, GF), and excellent conductivity. Hence, SA/P(AM-co-AAc)/Ca^{2+}-2 sensors were chosen for further research.

Figure 4e shows $\Delta R/R_0$ of the SA/P(AM-*co*-AAc)/Ca^{2+}-2 sensors during cyclic stretching-releasing tests with large strains (100–500%). Depending on the different responses produced by different strains, the hydrogel sensors could detect strains sensitively. Meanwhile, the $\Delta R/R_0$ remained stable under repeated stretching processes of the same strain, revealing the excellent stability and reproducibility of the hydrogel sensors. The response of the sensors to small strains (10–50%) is presented in Fig. S2. A similar phenomenon was found. As shown in Fig. 4f, the $\Delta R/R_0$ values of the SA/P(AM-*co*-AAc)/Ca^{2+}-2 sensors for 1000 stretching-releasing cycles under 100% strain remained stable, indicating outstanding cyclic stability, fabulous durability of hydrogels.

Human motion detection of SA/P(AM-*co*-AAc)/Ca^{2+} sensors

To evaluate the performance of human motion detection of SA/P(AM-*co*-AAc)/Ca^{2+} sensors, the hydrogel sensors were fixed on a wrist joint to detect the wrist bending (Fig. 5a). The relative resistance changes of the hydrogel sensors increased as the wrist bent and decreased when the wrist recovered, which was caused by the stretch and release of the hydrogel sensors [35]. Hence, the hydrogel sensors could be used for detecting the movements of the wrists.

Furthermore, by fixing the SA/P(AM-*co*-AAc)/Ca^{2+} sensors on other joints (including the finger, knee, and elbow) (Fig. 5b–d), similar signals could also be obtained when the joints bent and recovered, which proved that the hydrogel sensors had potential applications for real-time movements monitoring of human body.

Touch recognition of SA/P(AM-*co*-AAc)/Ca^{2+} sensors

During compression and release, the conductive network structure changed (Fig. 6a). When the sensors were compressed, the cross-sectional area decreased and caused a decrease in resistance [34], while the resistance returned to its original state as the sensors were released. The surface of the SA/P(AM-*co*-AAc)/Ca^{2+} sensor was covered with glass plates, and the signal was transmitted through copper wires for touch detection (Fig. 6b). As illustrated in Fig. 6c, d, the strain sensor could detect signals generated by writing. It could respond to different Arabic numbers "1, 2, 4" and the English letters "t, s" by outputting different signals. When writing different letters, strengths and writing styles were different. Therefore, the strain sensor produced different compressions and output different signals.

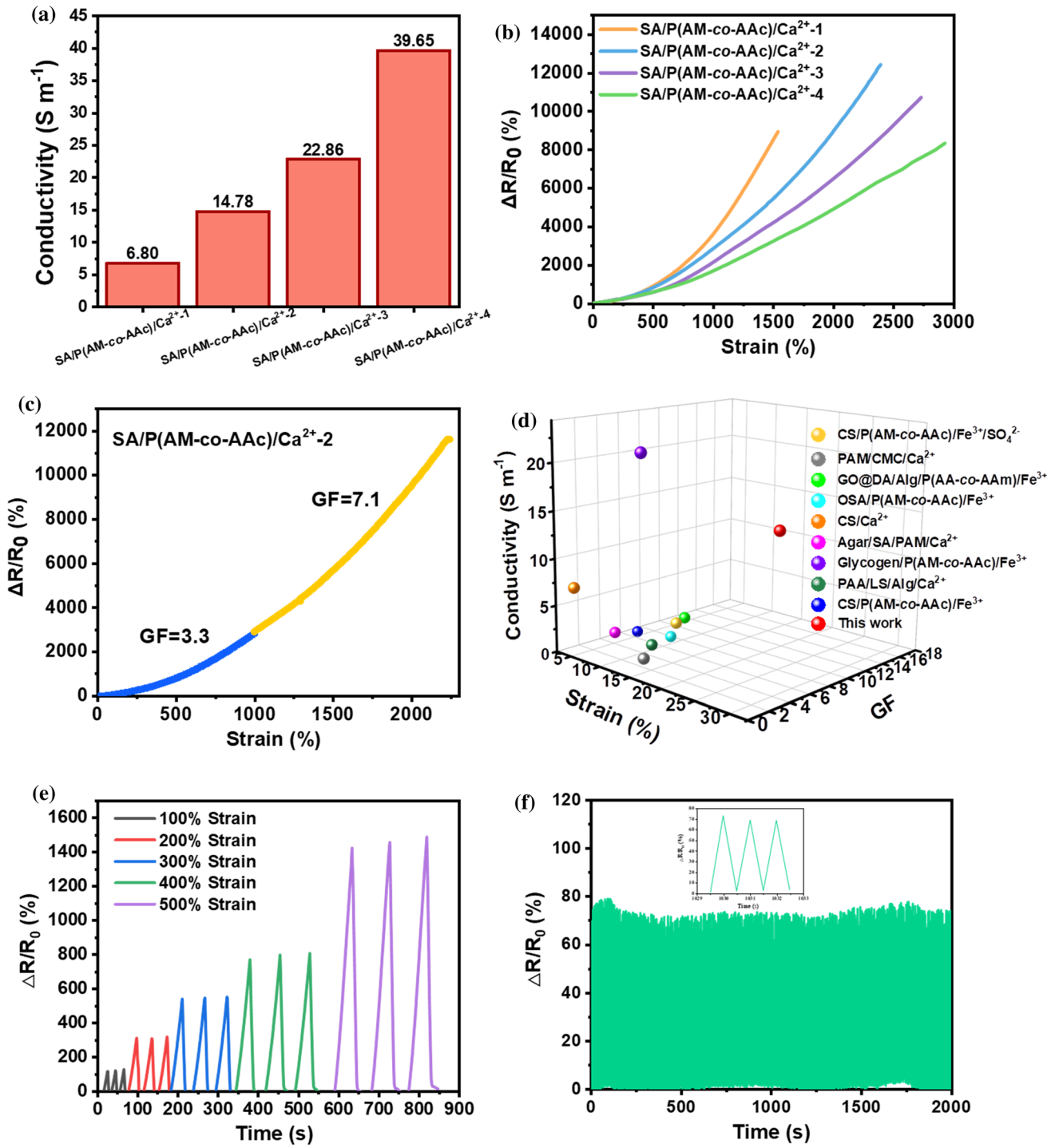

Figure 4 **a** Electrical conductivity and **b** $\Delta R/R_0$ at different strains of the SA/P(AM-*co*-AAc)/Ca^{2+} sensors, **c** $\Delta R/R_0$ at different strains of SA/P(AM-*co*-AAc)/Ca^{2+}-2 sensors, **d** comparison of elongation at break, conductivity and GF of hydrogel sensors in the reported literature, **e** $\Delta R/R_0$ of the SA/P(AM-*co*-AAc)/Ca^{2+}-2 sensors during cyclic stretching-releasing tests with large strains, **f** 1000 times (100% strain) stretching-releasing cycles of SA/P(AM-*co*-AAc)/Ca^{2+} sensors and the insert figure is the signal of an optional three cycles.

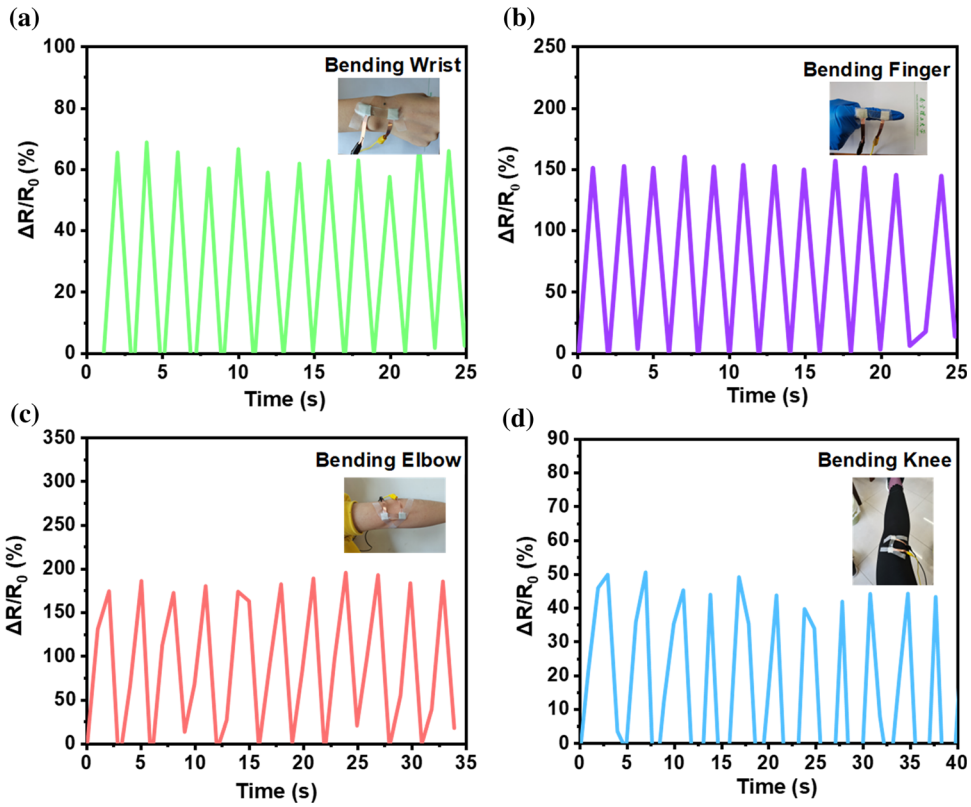

Figure 5 The $\Delta R/R_0$ of SA/P(AM-*co*-AAc)/Ca^{2+} sensors for detecting various physical movements including bending **a** wrist, **b** finger, **c** elbow, **d** knee.

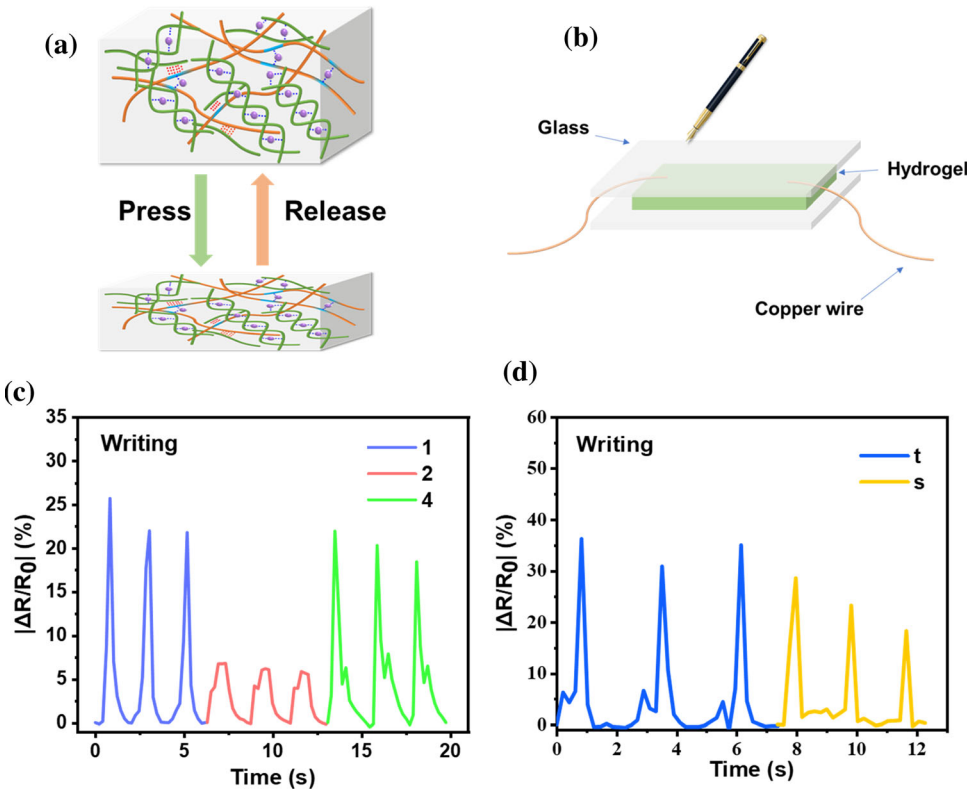

Figure 6 **a** Compression-release deformation of SA/P(AM-*co*-AAc)/Ca^{2+} hydrogels, **b** the structure of the strain sensor, changes in $\Delta R/R_0$ when writing **c** "1, 2, 4" and **d** "t, s".

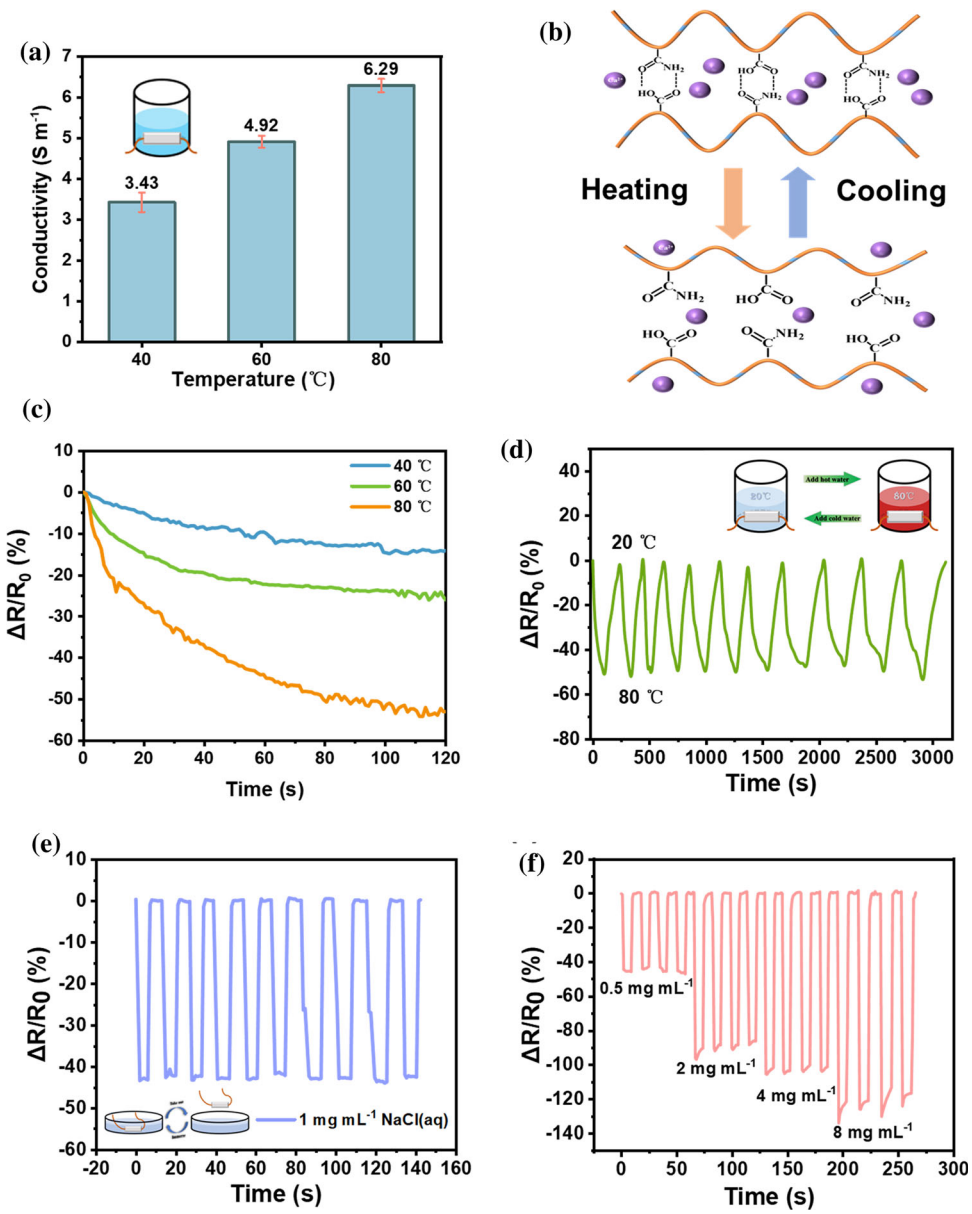

Figure 7 **a** Conductivity of SA/P(AM-*co*-AAc)/Ca^{2+} sensors at different temperatures, **b** structural change of the P(AM-*co*-AAc) upon heating/cooling cycle, **c** $\Delta R/R_0$ at different temperatures, **d** $\Delta R/R_0$ to cyclic 20 ~ 80 °C process, response of the SA/P(AM-*co*-AAc)/Ca^{2+} sensors to **e** cyclic immersion and removal in the NaCl solution of 1 mg mL^{-1} and **f** NaCl solutions with different concentrations (0.5, 2, 4, 8 mg $mL.^{-1}$).

Physiological environment detection of SA/P(AM-*co*-AAc)/Ca^{2+} sensors

The temperature response of the hydrogel sensors was tested by attaching the hydrogel sensors to the outer wall of the beaker with adhesive tapes and adding water of different temperatures into the beaker. As illustrated in Fig. 7a, the conductivity of SA/P(AM-*co*-AAc)/Ca^{2+} increased with the increase in temperatures. It could be attributed to the fact that P(AM-*co*-AAc) chains, featured as thermo-sensibility, present different conformations at different temperatures (Fig. 7b) [14]. At low temperatures, P(AM-*co*-AAc) chains contracted by reason of the formation of hydrogen bonds, which limited the migration of Ca^{2+} and decreased the conductivity, whereas hydrogen bonds were disrupted at high temperatures and the transport of Ca^{2+} became faster, thus improving the conductivity of the sensors. Figure 7c displays the $\Delta R/R_0$ of strain sensors under different temperatures. It could be seen that when the temperature rose from 40 to 80 °C, the changes of $\Delta R/R_0$ became greater. And this could also be owing to the faster ions transport in higher temperatures.

The response of strain sensors to temperature changes is displayed in Fig. 7d. $\Delta R/R_0$ values of the sensors dropped as the temperature increased from

20 to 80 °C, while increased as the temperature decreased from 80 to 20 °C. This is because the thermal motion of free ions was intense at high temperatures [36, 37]. A similar phenomenon was found by changing the temperature from 0 to 20 °C (Fig. S3). The output signals of the SA/P(AM-*co*-AAc)/Ca^{2+} sensors remained stable after several temperature conversion processes, implying that the hydrogel sensors possessed great reproducibility.

1 mg mL^{-1} NaCl solution was used to simulate sweat to test the response of SA/P(AM-*co*-AAc)/Ca^{2+} hydrogel sensors. Figure 7e illustrates the $\Delta R/R_0$ values of the sensors during cyclic immersion and removal in the NaCl solution. The resistance of the sensors decreased when immersed in NaCl solution, and returned to normal upon removal. After immersion in NaCl solution, the hydrogels swelled due to the electrostatic repulsion (caused by ionization of P(AM-*co*-AAc)) and promoted the migration of free ions [14]. Beyond this, the participation of NaCl solution introduced more free ions and improved the conductivity [38]. Notably, the electrical signals exhibited great stability and repeatability. Figure 7f exhibits the response of the sensors to different concentrations (0.5, 2, 4, 8 mg mL^{-1}) of NaCl solutions. $\Delta R/R_0$ values became larger with the increase in concentrations. Higher concentrations of NaCl solutions introduced more conductive ions, which enhanced the response of the hydrogel sensors [39].

pH response of SA/P(AM-*co*-AAc)/Ca^{2+} sensors

As a functional polymer, P(AM-*co*-AAc) is sensitive to pH changes [40]. The response of the SA/P(AM-*co*-AAc)/Ca^{2+} sensors to the different pH values is shown in Fig. 8a. When the sensors were immersed in an acidic medium (pH = 4), the $\Delta R/R_0$ decreased by 50%. There was a similar finding in an alkaline medium (pH = 9, the $\Delta R/R_0$ decreased by 30%). The amide groups of P(AM-*co*-AAc) accepted the protons and were positively charged when immersed in an acidic medium (Fig.S4(a)), causing the expansion of the polymer chains and swell of the hydrogels [41]. It promoted the transportation of free ions and reduced the resistance. While the hydrogel sensors were immersed in an alkaline medium, a similar phenomenon was found because carboxyl groups lost protons and were converted to $–COO^-$ (Fig. S4b) [42]. When the hydrogel sensors were removed from the acidic or alkaline medium, the resistance returned to its original state. Furthermore, the response to the pH changes was reversible and remained stable under multiple cycles [43–45].

Organic solvent response of SA/P(AM-*co*-AAc)/Ca^{2+} sensors

Figure 8b illustrates the response of the SA/P(AM-*co*-AAc)/Ca^{2+} sensors to different organic solvents (methanol, ethanol). When soaked in the organic solvents, the hydrogels showed swelling behavior and promoted migration of free ions, thus reducing the resistance of the sensors. When separated from the organic solvent, the resistance of the sensors returned to its original state for some time due to the deswelling process. Because the swelling rate of the SA/P(AM-*co*-AAc)/Ca^{2+} hydrogels varied in different organic solvents, the response of the sensors changed along with the polarity changes of organic solvents. Therefore, the SA/P(AM-*co*-AAc)/Ca^{2+} sensors could be used to distinguish the polarity of different organic solvents.

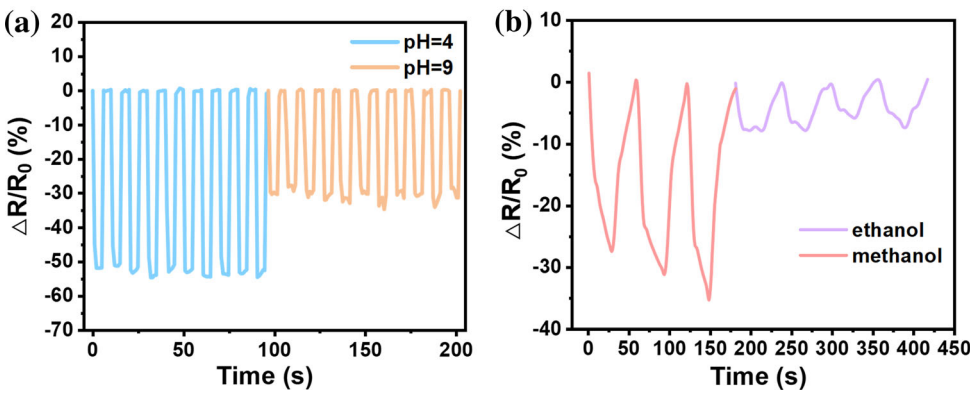

Figure 8 $\Delta R/R_0$ to different **a** pH values, **b** organic solvents.

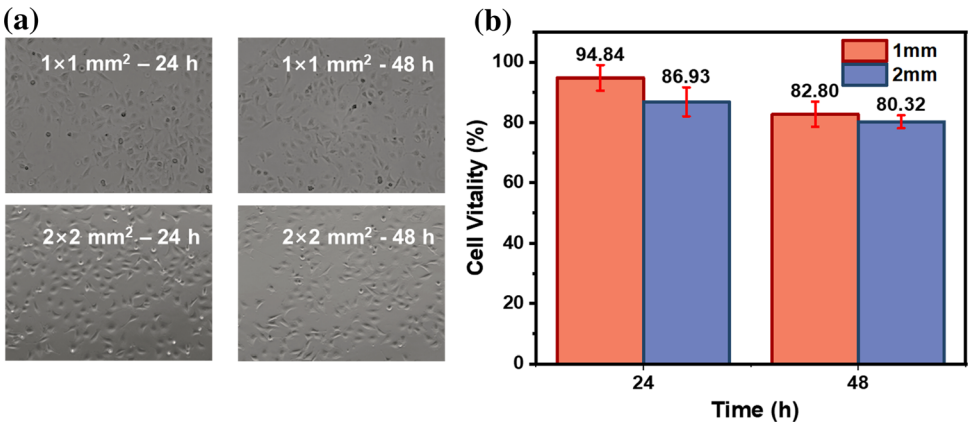

Figure 9 **a** Photographs of HUVEC cells inoculated on SA/P(AM-*co*-AAc)/Ca^{2+}, **b** cell viability in SA/P(AM-*co*-AAc)/Ca^{2+} hydrogels after 24 h and 48 h incubation.

Biocompatibility of SA/P(AM-*co*-AAc)/Ca^{2+} sensors

It is critical for wearable sensors to possess great biocompatibility because the sensors are directly attached to human skin. By inoculating HUVEC cells on the surface of the hydrogels with different sizes (1 × 1 mm^2, 2 × 2 mm^2) and observing their growth after 24 h and 48 h with the microscope (Fig. 9a), the biocompatibility of the hydrogel sensors was evaluated by the vitality of HUVEC cells. After 24 h and 48 h, the vitality of HUVEC cells remained relatively high with a slight decrease. Figure 9b shows that HUVEC cells inoculated on hydrogel surfaces maintained high vitality (above 80%) after 48 h. A piece of hydrogel was also placed on the skin for 24 h and then removed, and no allergies occurred (Fig. S5). Therefore, SA/P(AM-*co*-AAc)/Ca^{2+} hydrogels displayed excellent biocompatibility for the preparation of skin-friendly wearable sensors.

Conclusion

In summary, we prepared a highly stretchable, multifunctional, and biocompatible sensor consisting of SA, P(AM-*co*-AAc), and $CaCl_2$ hydrogel via a two-step method of polymerization and soaking. Double-network structure was constructed by the crosslinking of Ca^{2+} with SA and copolymer chains. The hydrogels exhibited outstanding stretchability of 2626% and extraordinary durability (1000 stretching-releasing cycles). The high sensitivity (gauge factor of 7.1) of the strain sensors was attributed to the introduction of Ca^{2+}. The characteristic of P(AM-*co*-AAc) enabled the sensors to respond to multi-stimuli (physiological environments and pH). The SA/P(AM-*co*-AAc)/Ca^{2+} sensors were capable of detecting real-time physical movements, touch, physiological changes, pH changes, and organic solvents accurately. In addition, the prepared hydrogels were biocompatible and displayed fabulous compatibility for HUVEC cells, revealing that the hydrogel sensors can be utilized as human-friendly wearable devices for human–computer interaction, health monitoring, and implanted in bio-electronics.

Acknowledgements

This work was supported by the National Undergraduate Training Program for Innovation and Entrepreneurship (202110288103).

Author contributions

YZ contributed to conceptualization, methodology, data curation, software, writing—original draft, writing—review and editing. TD contributed to methodology, data curation, and writing—review and editing. YC contributed to methodology, data curation, software,and writing—review and editing. QD contributed to methodology, data curation, and investigation. HW contributed to methodology, data curation, and software. WH contributed to methodology, data curation, and software. XL contributed to conceptualization, methodology, and data curation. HJ contributed to supervision, resources, project administration, and writing—review and editing.

Declarations

Conflict of interest The authors declare that they have no known competing financial interests or paper.

Supplementary Information: The online version contains supplementary material available at https://doi.org/10.1007/s10853-022-07635-5.

References

[1] Liu X, Wei Y, Qiu Y (2021) Advanced flexible skin-like pressure and strain sensors for human health monitoring. Micromachines. https://doi.org/10.3390/mi12060695

[2] Han F, Li M, Ye H, Zhang G (2021) Materials, electrical performance, mechanisms, applications, and manufacturing approaches for flexible strain sensors. Nanomaterials. https://doi.org/10.3390/nano11051220

[3] Wang S, Sun Z, Zhao Y, Zuo L (2021) A highly stretchable hydrogel sensor for soft robot multi-modal perception. Sens Actuators A-Phys. https://doi.org/10.1016/j.sna.2021.113006

[4] Shih B, Christianson C, Gillespie K, Lee S, Mayeda J, Huo Z, Tolley MT (2019) Design considerations for 3D printed soft, multimaterial resistive sensors for soft robotics. Front Robot AI 6:30–30. https://doi.org/10.3389/frobt.2019.00030

[5] G. Gang, H. Wei, S. Jinjun, D. Xiaochen (2018) Recent progress of flexible and wearable strain sensors for human-motion monitoring, Journal of Semiconductors, 39, 011012 (011021 pp.)-011012 (011021 pp.). https://doi.org/10.1088/1674-4926/39/1/011012.

[6] Wu X, Han Y, Zhang X, Zhou Z, Lu C (2016) Large-area compliant, low-cost, and versatile pressure-sensing platform based on microcrack-designed carbon black@polyurethane sponge for human-machine interfacing. Adv Func Mater 26:6246–6256. https://doi.org/10.1002/adfm.201601995

[7] Li G, Li C, Li G, Yu D, Song Z, Wang H, Liu X, Liu H, Liu W (2022) Development of conductive hydrogels for fabricating flexible strain sensors. Small. https://doi.org/10.1002/smll.202101518

[8] Tang L, Wu S, Qu J, Gong L, Tang J (2020) A review of conductive hydrogel used in flexible strain sensor. Materials. https://doi.org/10.3390/ma13183947

[9] Wang Z, Cong Y, Fu J (2020) Stretchable and tough conductive hydrogels for flexible pressure and strain sensors. J Mater Chem B 8:3437–3459. https://doi.org/10.1039/c9tb02570g

[10] Tie J, Rong L, Liu H, Wang B, Mao Z, Zhang L, Zhong Y, Feng X, Sui X, Xu H (2020) An autonomously healable, highly stretchable and cyclically compressible, wearable hydrogel as a multimodal sensor. Polym Chem 11:1327–1336. https://doi.org/10.1039/C9PY01737B

[11] Liu X, Ren Z, Liu F, Zhao L, Ling Q, Gu H (2021) Multifunctional self-healing dual network hydrogels constructed via host-guest interaction and dynamic covalent bond as wearable strain sensors for monitoring human and organ motions. ACS Appl Mater Interfaces 13:14625–14635. https://doi.org/10.1021/acsami.1c03213

[12] Xia M, Pan S, Li H, Yi X, Zhan Y, Sun Z, Jiang X, Zhang Y (2021) Hybrid double-network hydrogel for highly stretchable, excellent sensitive, stabilized, and transparent strain sensors. J Biomater Sci-Polym Ed 32:1548–1563. https://doi.org/10.1080/09205063.2021.1922170

[13] Hong X, Ding H, Li J, Xue Y, Sun L, Ding F (2021) Poly(acrylamide-co-acrylic acid)/chitosan semi-interpenetrating hydrogel for pressure sensor and controlled drug release. Polym Adv Technol 32:3050–3058. https://doi.org/10.1002/pat.5317

[14] Li X, Wang J, Lin Y, Cheng Y, Han W, Yuan G, Jia H (2022) High-strength, biocompatible and multifunctional hydrogel sensor based on dual physically cross-linked network. Colloids Surfaces A-Physicochem Eng Aspects. https://doi.org/10.1016/j.colsurfa.2021.128091

[15] Liang B, Zhao H, Zhang Q, Fan Y, Yue Y, Yin P, Guo L (2016) Ca^{2+} Enhanced nacre-inspired montmorillonite-alginate film with superior mechanical transparent, fire retardancy, and shape memory properties. Acs Appl Mater Interfaces 8:28816–28823. https://doi.org/10.1021/acsami.6b08203

[16] Wang T, Wang J, Li Z, Yue M, Qing X, Zhang P, Liao X, Fan Z, Yang S (2022) PVA/SA/MXene dual-network conductive hydrogel for wearable sensor to monitor human motions. J Appl Polym Sci 139:51627

[17] Wang M, Zang Y, Hong K, Zhao X, Yu C, Liu D, An Z, Wang L, Yue W, Nie G (2021) Preparation of pH-sensitive carboxymethyl cellulose/chitosan/alginate hydrogel beads with reticulated shell structure to deliver Bacillus subtilis natto. Int J Biol Macromol 192:684–691. https://doi.org/10.1016/j.ijbiomac.2021.10.019

[18] Feng K, Hung GY, Yang X, Liu M (2019) High-strength and physical cross-linked nanocomposite hydrogel with clay nanotubes for strain sensor and dye adsorption application. Comp Sci Technol. https://doi.org/10.1016/j.compscitech.2019.107701

[19] Wang H, Wan Y, Wang W, Li W, Zhu J (2018) Effect of calcium ions on the III steps of self-assembly of SA investigated with atomic force microscopy. Int J Food Prop 21:1995–2006. https://doi.org/10.1080/10942912.2018.1494200

[20] Zhu E, Xu H, Xie Y, Song Y, Liu D, Gao Y, Shi Z, Yang Q, Xiong C (2021) Antifreezing ionotronic skin based on flexible, transparent, and tunable ionic conductive nanocellulose hydrogels. Cellulose 28:5657–5668. https://doi.org/10.1007/s10570-021-03878-8

[21] Sun H, Zhou K, Yu Y, Yue X, Dai K, Zheng G, Liu C, Shen C (2019) Highly stretchable, transparent, and bio-friendly strain sensor based on self-recovery ionic-covalent hydrogels for human motion monitoring. Macromol Mater Eng. https://doi.org/10.1002/mame.201900227

[22] Wang T, Ren X, Bai Y, Liu L, Wu G (2021) Adhesive and tough hydrogels promoted by quaternary chitosan for strain sensor. Carbohydr Polym. https://doi.org/10.1016/j.carbpol.2020.117298

[23] Chen D, Zhao X, Gao H, Ren G, Luo J, Wang H, Zha C, Yang K, Jia P (2022) High-strength conductive, antifouling, and antibacterial hydrogels for wearable strain sensors. ACS Biomater Sci Eng 8:2624–2635. https://doi.org/10.1021/acsbiomaterials.1c01630

[24] Ding F, Wu S, Wang S, Xiong Y, Li Y, Li B, Deng H, Du Y, Xiao L, Shi X (2015) A dynamic and self-crosslinked polysaccharide hydrogel with autonomous self-healing ability. Soft Matter 11:3971–3976. https://doi.org/10.1039/C5SM00587F

[25] Wang J, Lin Y, Mohamed A, Ji Q, Jia H (2021) High strength and flexible aramid nanofiber conductive hydrogels for wearable strain sensors. J Mater Chem C 9:575–583. https://doi.org/10.1039/d0tc02983a

[26] Liang Y, Ye L, Sun X, Lv Q, Liang H (2020) Tough and stretchable dual ionically cross-linked hydrogel with high conductivity and fast recovery property for high-performance flexible sensors. ACS Appl Mater Interfaces 12:1577–1587. https://doi.org/10.1021/acsami.9b18796

[27] Bai J, Wang R, Wang X, Liu S, Wang X, Ma J, Qin Z, Jiao T (2021) Biomineral calcium-ion-mediated conductive hydrogels with high stretchability and self-adhesiveness for sensitive iontronic sensors. Cell Rep Phys Sci. https://doi.org/10.1016/j.xcrp.2021.100623

[28] Jin X, Jiang H, Zhang Z, Yao Y, Bao X, Hu Q (2021) Ultrastretchable, self-adhesive, strain-sensitive and self-healing GO@DA/Alginate/P(AAc-*co*-AAm) multifunctional hydrogels via mussel-inspired chemistry. Carbohydr Polym 254:117316. https://doi.org/10.1016/j.carbpol.2020.117316

[29] Wang J, Dai T, Lin Y, Jia H, Ji Q, Yuan G (2022) Polysaccharide-based high-strength, self-healing and ultrasensitive wearable sensors. Ind Crops Prod. https://doi.org/10.1016/j.indcrop.2022.114618

[30] Wang X, Chen G, Tian J, Wan X (2022) Chitin/Ca solvent-based conductive and stretchable organohydrogel with anti-freezing and anti-drying. Int J Biol Macromol 207:484–492. https://doi.org/10.1016/j.ijbiomac.2022.03.025

[31] Wang J, Liu Y, Su S, Wei J, Rahman SE, Ning F, Christopher G, Cong W, Qiu J (2019) ultrasensitive wearable strain sensors of 3D printing tough and conductive hydrogels. Polym (Basel). https://doi.org/10.3390/polym11111873

[32] Hussain I, Ma X, Luo Y, Luo Z (2020) Fabrication and characterization of glycogen-based elastic, self-healable, and conductive hydrogels as a wearable strain-sensor for flexible e-skin. Polymer. https://doi.org/10.1016/j.polymer.2020.122961

[33] Fu C, Yi Y, Lin J, Kong F, Chen L, Ni Y, Huang L (2022) Lignin reinforced hydrogels with fast self-recovery, multifunctionalities via calcium ion bridging for flexible smart sensing applications. Int J Biol Macromol 200:226–233. https://doi.org/10.1016/j.ijbiomac.2021.12.102

[34] Liu H, Wang X, Cao Y, Yang Y, Yang Y, Gao Y, Ma Z, Wang J, Wang W, Wu D (2020) Freezing-tolerant highly sensitive strain and pressure sensors assembled from ionic conductive hydrogels with dynamic cross-links. Acs Appl Mater Interfaces 12:25334–25344. https://doi.org/10.1021/acsami.0c06067

[35] Gao Y, Gu S, Jia F, Wang Q, Gao G (2020) "All-in-one" hydrolyzed keratin protein-modified polyacrylamide composite hydrogel transducer. Chem Eng J. https://doi.org/10.1016/j.cej.2020.125555

[36] Yan Y, Wei L, Qiu X, Shao J, Liu H, Cui X, Huang J, Xie L, Hu Z, Huang C, Dual-Responsive A (2021) Freezing-tolerant hydrogel sensor and related thermal- and strain-sensitive mechanisms. Acs Appl Polym Mater 3:1479–1487. https://doi.org/10.1021/acsapm.0c01346

[37] Feng S, Li Q, Wang S, Wang B, Hou Y, Zhang T (2019) Tunable dual temperature-pressure sensing and parameter self-separating based on ionic hydrogel via multisynergistic network design. ACS Appl Mater Interfaces 11:21049–21057. https://doi.org/10.1021/acsami.9b05214

[38] Jiang X, Xiang N, Zhang H, Sun Y, Lin Z, Hou L (2018) Preparation and characterization of poly(vinyl alcohol)/sodium alginate hydrogel with high toughness and electric conductivity. Carbohyd Polym 186:377–383. https://doi.org/10.1016/j.carbpol.2018.01.061

[39] Huang H, Han L, Fu X, Wang Y, Yang Z, Pan L, Xu M (2020) Multiple stimuli responsive and identifiable zwitterionic ionic conductive hydrogel for bionic electronic skin. Adv Electron Mater. https://doi.org/10.1002/aelm.202000239

[40] Wang LP, Ren J, Yao MQ, Yang XC, Yang W, Li Y (2014) Synthesis and characterization of self-oscillating P(AA-co-AM)/PEG semi-IPN hydrogels based on a pH oscillator in

closed system. Chin J Polym Sci 32:1581–1589. https://doi.org/10.1007/s10118-014-1552-4

[41] Pathak AK, Singh VK (2017) A wide range and highly sensitive optical fiber pH sensor using polyacrylamide hydrogel. Opt Fiber Technol 39:43–48. https://doi.org/10.1016/j.yofte.2017.09.022

[42] Chen YH, He YC, Yaung JF (2014) Exploring pH-sensitive hydrogels using an ionic soft contact lens: an activity using common household materials. J Chem Educ 91:1671–1674. https://doi.org/10.1021/ed400833b

[43] E.M. S, K.L. O, G.V. O (1999) The effect of external stimuli on the equilibrium swelling properties of poly (N-vinyl 2-pyrrolidone/itaconic acid) poly-electrolyte hydrogels, Polymer, 40, 913–917.

[44] Fei JQ, Gu LX (2002) PVA/PAA thermo-crosslinking hydrogel fiber: preparation and pH-sensitive properties in electrolyte solution. Eur Polymer J 38:1653–1658. https://doi.org/10.1016/S0014-3057(02)00032-0

[45] Zhang YX, Wu FP, Li MZ, Wang EJ (2005) pH switching on-off semi-IPN hydrogel based on cross-linked poly(acrylamide-co-acrylic acid) and linear polyallyamine. Polymer 46:7695–7700. https://doi.org/10.1016/j.polymer.2005.05.121